Article

S100A12 triggers NETosis to aggravate myocardial infarction injury via the Annexin A5-calcium axis

Xi Zhang[1,2], Haixu Song[1,2], Dan Liu[1], Yi Cai[1], Ziqi Liu[1], Xiaolin Zhang[1], Xiaojie Zhao[1], Yan Zhang[1], Quanmin Jing[1], Chenghui Yan [1] ✉ & Yaling Han [1] ✉

Neutrophil extracellular traps (NETs) play a critical role in acute myocardial infarction (AMI) and the externalization of S100 family members. Here, we show the effects of S100A12 on NETs formation and myocardial injury following AMI. S100A12 expression increases rapidly in neutrophils and peaks on day 1 after AMI, promoting NETs production and exacerbating myocardial injury. DNase I, an inhibitor of NETs, reduces apoptosis of cardiomyocytes induced by S100A12. Mechanistically, the interaction of S100A12 and Annexin A5 (ANXA5) enhances calcium influx and promotes NETs formation. Blockage of ANXA5 effectively attenuates heart function impairment after AMI. Finally, we show that plasma S100A12 levels correlate with dsDNA concentration, and this correlation is associated with an increased risk of all-cause mortality during the 1-year follow-up of AMI patients. These findings, derived from male mice, reveal the S100A12-ANXA5-calcium influx axis as a potential therapeutic target and biomarker for AMI.

Although improvements in percutaneous coronary intervention have greatly reduced the mortality rate of acute myocardial infarction (AMI) patients, the prevalence of heart failure remains increasing. Affected patients tend to have more comorbidities, worsening economic strain on healthcare systems and impeding effective medical management[1]. Once AMI occurs, cardiomyocytes show rapid ischemic damage, which plays a key role in the occurrence of long-term heart failure. Therefore, there is an urgent need to understand the mechanism of early ischemic injury in myocardial cells and identify therapeutic targets to improve the prognosis of AMI[2].

S100A12, a newly discovered member of the S100 family of calcium regulatory proteins, is located within the same gene cluster on chromosome 1q21 as other S100A family members[3]. In humans, S100A12 is mainly secreted by neutrophils and monocytes[4], but can also be expressed by tissue cells, such as mucosal epithelial cells and keratinocytes. Rodents do not express S100A12[5]. The upregulation of S100A12 is primarily driven by cellular stress, which induces its release from granulocytes and other myeloid cells. Upon release, S100A12 binds to its canonical receptor, RAGE, which engages the extracellular

domain of this target protein via calcium-bound S100A12. Cumulative studies have demonstrated that S100A12 is associated with many inflammatory, metabolic diseases and cardiovascular events in atherosclerotic diseases[6,7]. Based on analyses in multivariate Cox proportional hazard models, the S100A12 protein level in peripheral blood has been identified as an independent predictor of major adverse cardiovascular events in patients with stable coronary artery disease[8]. Our previous study revealed that S100A12 is a potential biomarker for the early diagnosis and prediction of ST-segment elevation myocardial infarction (STEMI)[9]. Recent single-cell sequencing studies showed that S100A12 may serve as a biomarker for neutrophil screening, and can be used for the isolation and analysis of neutrophil subpopulations[10]. However, it is unclear whether S100A12 contributes to the occurrence and prognosis of AMI through the regulation of neutrophils.

Neutrophils are the earliest immune cells recruited to the ischemic heart after AMI and are responsible for maintaining the initial acute proinflammatory response to AMI injury[11]. The level of neutrophils in AMI patients positively correlates with the size of the MI, cardiac dysfunction, and adverse clinical outcome[12,13]. Moreover, their

[1]State Key Laboratory of Frigid Zone Cardiovascular Disease, Cardiovascular Research Institute and Department of Cardiology, General Hospital of Northern Theater Command, Shenyang 110016, China. [2]These authors contributed equally: Xi Zhang, Haixu Song. ✉e-mail: yanch1029@163.com; hanyaling@163.net

rapid degradation and degranulation lead to the spread of inflammation into the adjacent area of the infarcted tissue and trigger the infiltration of monocytes. A key feature of neutrophils is the release of neutrophil extracellular traps (NETs)[14]. NETs were first described in 2004 by Brinkmann and colleagues, who documented the expulsion of extracellular webbed structures comprising chromatin and histones, studded with neutrophil granule proteins[15]. The process of NET release (NETosis) is initiated by granular proteins such as myeloperoxidase (MPO), neutrophil elastase (NE), and peptidylarginine deiminase 4 (PAD4). PAD4 mediates the citrullination of histone 3 (citH3), inducing chromatin decondensation before extracellular release[16].

In this study, we constructed transgenic mice with myeloid-specific overexpression of human S100A12 and evaluated the effects of S100A12 on the occurrence and prognosis of AMI in mice, as well as the molecular mechanisms underlying NETosis.

Results

Myocardial injury is aggravated in the transgenic (TG) mouse model with myeloid specific expression of humanized S100A12 after MI

We generated a TG mouse model expressing human S100A12 in a myeloid-specific manner (Supplementary Fig. 1a, b). We found that S100A12 was highly expressed in bone marrow-derived neutrophils (BMDNs) than in spleen-derived neutrophils of TG mice (Supplementary Fig. 1c, d). Next, left anterior descending (LAD) coronary artery ligation was performed in both TG and wild-type (WT) mice. Cardiac function was analysed on Day 28 post-MI (Fig. 1a). Echocardiography data showed that the percentage of ejection fraction (EF) and fractional shortening (FS) were significantly decreased in TG mice compared to WT controls (Fig. 1b, c). Consistently, the left ventricle (LV) anterior wall became thinner ($P = 0.0005$) (Fig. 1d–i). Hematoxylin & eosin and Masson staining showed a larger scar size and a higher proportion of fibrosis in TG mice than in WT mice 28 days after ligation (Fig. 1j–l). Taken together, these findings indicate that S100A12 expression worsens cardiac function and ventricular remodelling under MI.

S100A12 enhances NETs, and aggravates apoptosis of heart tissue at the early stage following MI

We next showed that the expression of S100A12 was increased rapidly, reaching its peak level on Day 1 after MI and progressively decreasing in the border area of the heart tissue in TG mice (Fig. 2a–e). Co-immunofluorescence staining showed that the number of Ly6G-positive neutrophils increased significantly at the edge of the infarcted tissue on Day 1 post-MI in TG mice compared with that in WT mice ($P = 0.0014$) (Fig. 2f–h). Moreover, we showed that S100A12 was mainly expressed in Ly6G-positive neutrophils in TG mice (Fig. 2f–h).

To further investigate the effect of S100A12 on neutrophils post-MI, we examined NETs production in the infarcted myocardial tissue. We found that the protein levels of NE, MPO, and citH3 were significantly higher in the TG-MI group than in the WT-MI group ($P = 0.0277$ for NE and $P = 0.0396$ for citH3) (Fig. 2i, j). Immunohistochemical (IHC) staining for citH3, MPO, and NE confirmed that the expression of these proteins was considerably higher in the border area of the infarcted tissue in TG mice than in WT mice on day 1 after MI (Fig. 2k–n).

Apoptosis is a major cause of cardiac impairment during early MI. To evaluate whether S100A12 aggravates myocardial apoptosis, we examined the expression of Cleaved-caspase 3, Caspase 3, Bax, and Bcl2 on Day 1 post MI. Western blotting revealed that MI injury led to an increase in the ratios of Bax/Bcl2 and Cleaved-caspase3/Caspase3 in TG mice compared with those in WT mice (Supplementary Fig. 2a, b). The expression of Cleaved-caspase 3 in the border area of the infarcted tissue, as detected by IHC staining, was consistent with the western blotting results (Supplementary Fig. 2c, d). These findings indicate that

S100A12 contributes to NETs production, which may aggravate cardiomyocyte apoptosis after MI.

Blockage of NETs production mitigates S100A12-induced cardiomyocyte apoptosis and cardiac dysfunction in TG mice

Next, we asked whether myocardial injury is caused by S100A12-induced NET formation. To address this question, we intraperitoneally injected DNase I for 3 days, a classical inhibitor of NETs (Supplementary Fig. 3a). The expression of NETs markers in DNase I-injected mice was significantly lower than that in saline-injected mice in both the TG and WT groups on Day 1 after MI (Supplementary Fig. 3b–e). Meanwhile, the ratios of Bax/Bcl$_2$ and Cleaved-caspase3/Caspase3 in DNase I-injected mice were lower. This reduction was more significant in the TG group, which was associated with decreased NETs formation (Supplementary Fig. 3f–h). Moreover, TdT-mediated dUTP Nick-End Labelling (TUNEL) staining established that treatment with DNase I significantly decreased the proportion of apoptotic cardiomyocytes after MI in both TG and WT groups (Supplementary Fig. 3i, j). Echocardiographic analyses revealed that TG mice treated with DNase I showed some improvement in the percentage of EF and FS on Day 28 post-MI compared with saline-injected mice as showed in Supplementary Fig. 3k, l. Similarly, H&E and Masson staining showed that the DNase I injected mice experienced obviously reduced infarct size and wall thickness compared with that in corn oil-injected TG mice, though there was no significant difference between the WT groups (Supplementary Fig. 3m-q).

S100A12 promotes NETs formation in BMDNs ex vivo and in vitro

To further evaluate the role of S100A12 in NETs formation in ex vivo study, we extracted BMDNs from TG and WT mice, respectively. SYTOX Green staining showed that S100A12 expression stimulated neutrophils to produce more DNA reticular structures (Fig. 3a, b). Immunofluorescence staining (Fig. 3c, d) and western blotting (Fig. 3e, f) revealed that the expression of NETs components (citH3, NE, and MPO) and key enzymes (PAD4) was higher in S100A12-overexpressing neutrophils than in the control group.

Next, we overexpressed S100A12 in neutrophil-like differentiated HL-60 (dHL-60) cells, which exhibited immediate flattening, stronger cell adhesion, earlier appearance of intracellular vacuoles, higher plasma membrane permeability, and faster chromatin release compared with the control group (Fig. 3g). Similarly, the mRNA and protein levels of NET-related proteins (citH3, NE, MPO, and PAD4) were increased upon overexpression of S100A12 (Fig. 3h–j). Conversely, when S100A12 was inhibited by siRNA, the levels of these NETs markers were decreased (Fig. 3k–m). Collectively, our findings suggest that overexpression of S100A12 accelerates NETs formation in neutrophils in ex vivo and in vitro.

Overexpression of S100A12 in neutrophils exacerbates cardiomyocyte apoptosis by release of NETs in vitro

To investigate whether S100A12 expression in neutrophils controls cardiomyocyte apoptosis by releasing NETs, we created a co-culture system of dHL-60 neutrophils and HL-1 cardiomyocytes. The decrease and increase in S100A12 content in dHL-60 neutrophils were achieved by siRNA transfection and S100A12 plasmid overexpression, respectively. DNase I was added to dHL-60 neutrophils to inhibit NETs formation. Western blotting (Supplementary Fig. 4a–d) and TUNEL staining (Supplementary Fig. 4e–h) demonstrated that apoptosis of cardiomyocytes co-cultured with S100A12-low neutrophils was slightly reduced but significantly increased in S100A12-high neutrophils compared with that of the control group. Moreover, addition of DNase I reduced the level of cardiomyocyte apoptosis induced by co-cultured S100A12-high expression neutrophils to normal levels.
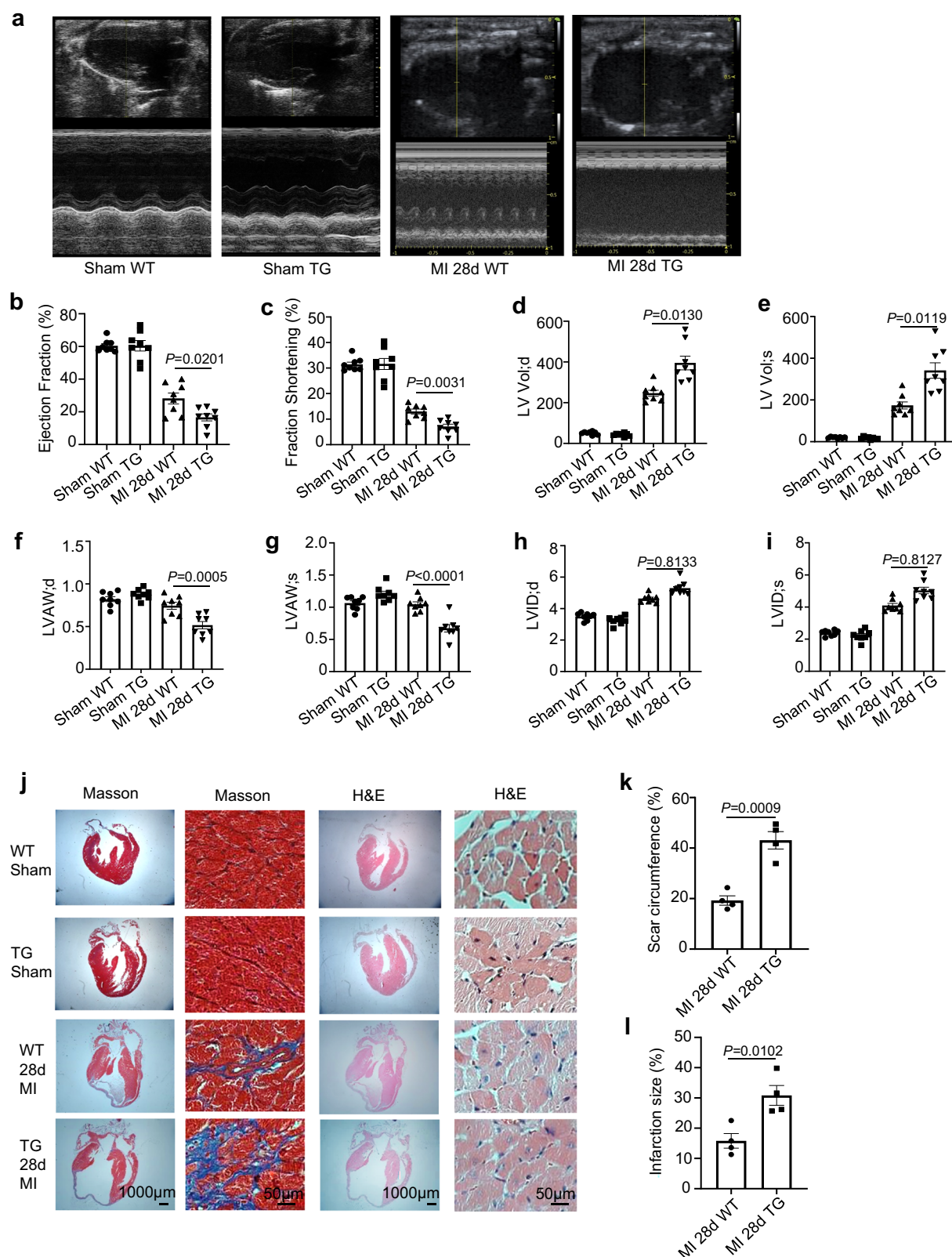
Fig. 1 | S100A12 expression aggravated myocardial infarction (MI) injury.
a Representative echocardiographic recordings at Day 28 after MI or sham operation. **b**–**i** Echocardiographic parameters were analyzed ($n = 8$ biological replicates). **j** Representative Masson and Hematoxylin & eosin and staining of cardiac tissue obtained from WT and TG mice at Day 28 after MI or sham operation. Quantitative analysis of scar circumference (**k**) and infarct size (**l**) at Day 28 post-MI in WT and TG mice ($n = 4$ biological replicates). Data are expressed as mean ± SEM. Statistical analyses were carried out using two-tailed unpaired *t*-test for (**k**), (**l**), one-way ANOVA with Tukey's multiple comparisons test for (**b**), (**f**), (**g**), Brown-Forsythe and Welch's ANOVA test for (**c**), (**d**), (**e**), and Kruskal-Wallis test with Dunn's multiple-comparison test for (**h**), (**i**). Source data are provided as a Source Data file.
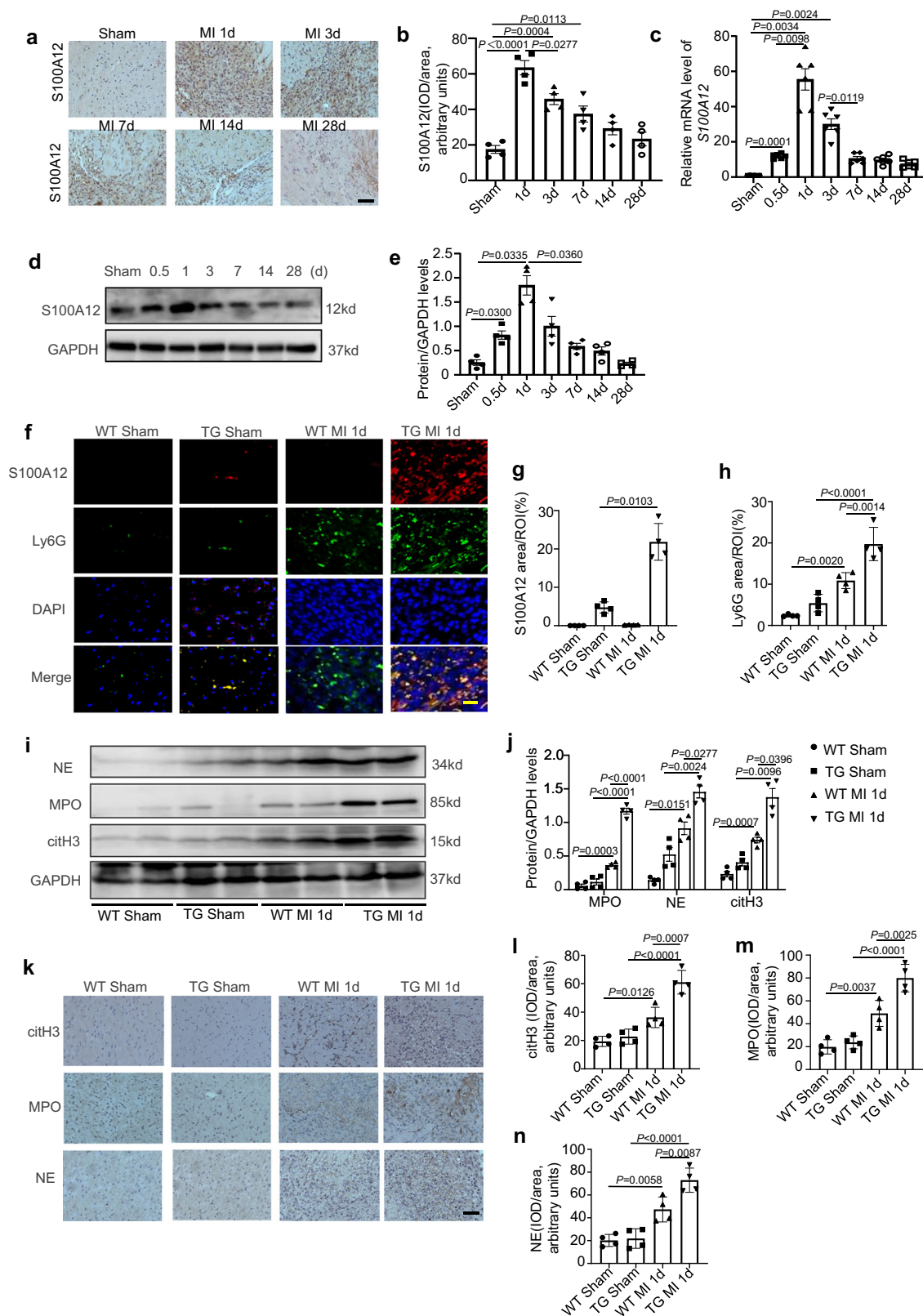
Endogenous S100A12 promotes suicide NETosis by the NADPH oxidase 4 (NOX4)-reactive oxygen species (ROS)-pERK pathway
To evaluate whether S100A12 directly regulates NETs formation, we treated neutrophils overexpressing S100A12 with different concentrations of Glibenclamide, an inhibitor of S100A12 release in a dose-dependent manner. We found that the expressions of NE, MPO, and citH3 dramatically increased in dHL-60 cells transfected with S100A12

overexpression plasmid (Supplementary Fig. 5a–c), although S100A12 secretion was inhibited. These results suggest that intracellular S100A12 initiates NETosis formation. Suicide NETosis is a common type of NETosis in aseptic inflammation, therefore, we detected whether S100A12 induced it occurred. The ratio of p-ERK/t-ERK was higher in TG mice-derived primary neutrophils compared to WT mice (Supplementary Fig. 6a, b). Induction of NETosis depends on ROS, the

Fig. 2 | Content of S100A12 significantly increased in the myocardial tissue of TG mice during the early stages after MI, in parallel to leukocyte infiltration and neutrophil extracellular traps (NETs) formation. a, b Representative immunohistochemical (IHC) staining of S100A12 and quantification in the border area of infarcted myocardial tissue of TG mice at different time points after MI ($n = 4$ biological replicates). Scale bar, 50 µm. **c** *S100A12* mRNA expression level was analyzed in the border area of TG mice at different time points after MI ($n = 6$ biological replicates). **d, e** Representative blots of S100A12 and quantitative analysis in the border area of TG mice at different time points after MI ($n = 4$ biological replicates). **f–h** Immunofluorescence double staining of neutrophil marker (Ly6G) and S100A12 in the border area of TG and WT mice and quantification at day 1 post-MI ($n = 4$ biological replicates). Scale bar, 20 µm. **i, j** Representative blots of NETs-related proteins [myeloperoxidase (MPO), neutrophil elastase (NE), and citrullination of histone 3 (citH3)] and quantification in WT and TG mice at Day 1 after MI or sham operation. One-way ANOVA with Tukey's multiple comparisons test is used for statistical analyses of MPO, Brown-Forsythe and Welch's ANOVA test is used for analyses of NE and citH3 ($n = 4$ biological replicates). **k–n** Representative IHC staining of NET-related proteins and quantification in WT and TG mice at Day 1 post-MI ($n = 4$ biological replicates). Scale bar, 50 µm. Data are expressed as mean ± SEM. Statistical analyses were carried out using one-way ANOVA with Tukey's multiple comparisons test for (**h**), (**l**), (**m**), (**n**) and Brown-Forsythe and Welch's ANOVA test for (**b**), (**c**), (**e**), (**g**). Source data are provided as a Source Data file.

main source of which is NADPH oxidase. Activation of NADPH oxidase depends on increase in the concentration of Ca^{2+} in the cytoplasm and in mitochondria. We observed that the overexpression of S100A12 in dHL-60 cells was associated with an enhanced superoxide production detected by dihydroethidium (DHE) and MitoSOX Red staining. In contrast, silence of S100A12 reduced the uperoxide production (Supplementary Fig. 6c–f). The addition of ROS inhibitor Diphenyleineideom (DPI) could reduce NETs formation in dHL-60 cells transfected with pcDNA3.1-S100A12 in a dose-dependent manner (Supplementary Fig. 6g, h). Further, we examined the correlation of several NADPH oxidase isoforms with S100A12 expression and found that S100A12 correlates more closely with NOX4 (Supplementary Fig. 6i–k).

Endogenous S100A12 increases the calcium overload in neutrophils

Previous studies have demonstrated that NETs release starts with the activation of surface receptors, followed by changes in intracellular calcium concentration[10]. Importantly, we found that there was a significant increase in Rhod2 intensity in cells transfected with pcDNA3.1-S100A12 ($P = 0.0219$), but a declining trend in si-S100A12 transfected cells compared to the control group (Fig. 4a, b), indicating that overexpression of S100A12 increases the intracellular calcium concentration in neutrophils. These findings were next confirmed by calcium colorimetric assay (Fig. 4c). Ionomycin is a potent selective calcium ionophore that regulates calcium influx and increases intracellular calcium ion levels by directly stimulating the calcium pool. Next, dHL-60 cells were preloaded with the Ca^{2+} dye Fluo-4 AM and activated with ionomycin. We then compared the cytosolic Ca^{2+} concentration at different time intervals based on the duration of stimulation. Results of the fluorescence spectrophotometry assays demonstrated that inhibition of S100A12 expression by siRNA reduced calcium influx in neutrophils compared to that in the control group (Fig. 4d, e). Furthermore, using different concentrations of Verapamil, a classical calcium-channel blocker, we showed a reduction of S100A12-induced NETs formation in a dose-dependent manner (Fig. 4f–j). Similarly, we performed MI in WT and TG mice with Verapamil administration before the MI surgery and on the Day 1 and Day 3 after MI (Supplementary Fig. 7a). The expression of MPO and citH3 in verapamil-injected TG mice was significantly lower than that in vehicle-injected TG mice on day 1 after MI (Supplementary Fig. 7b–g). Meanwhile, injection of Verapamil significantly improved the mortality rate in the acute phase after MI and cardiac function at 14 days post MI in TG mice (Fig. 4k–n).

Annexin A5(ANXA5) mediates S100A12-induced NETs formation

We went on to investigate how S100A12 regulates calcium overload in NETs formation. We used TMT quantitative proteomics to screen for differentially expressed proteins in tissues from WT and TG mice (Fig. 5a). Among the top five proteins, ANXA5 expression was the highest in TG mice than in WT mice at both mRNA and protein levels (Fig. 5b–d). Similarly, ANXA5 expression in dHL-60 cells was increased by the transfection of S100A12 overexpression plasmid and decreased with the silencing of S100A12 at both mRNA and protein levels

(Fig. 5e–g). Interestingly, ANXA5 overexpression increased NETs production although the expression of S100A12 was reduced, whereas ANXA5 silencing inhibited S100A12-induced NETs formation (Fig. 5h–o). SYTOX Green staining showed that overexpression of ANXA5 stimulated neutrophils to produce more reticular DNA structure, and blockage of ANXA5 significantly inhibited the occurrence of NETs (Fig. 5j, k). Taken together, our results suggest that ANXA5 mediates S100A12-induced NETs formation.

S100A12 interacts with ANXA5 to activate calcium overload in neutrophils

Next, we found that ANXA5 directly interacted with S100A12 in dHL-60 cells (Supplementary Fig. 8a). Moreover, immunofluorescence staining revealed significant co-localization of ANXA5 and S100A12 from the plasma to the cell membrane of dHL-60 cells after transfection with pcDNA3.1-S100A12 (Supplementary Fig. 8b–d). Since both ANXA5 and S100A12 are calcium-regulating proteins, we investigated whether the S100A12-ANXA5 interaction mediates calcium influx to induce NETs formation. We found that overexpression of ANXA5 remarkably increased the fluorescence intensity of Rhod2 in dHL-60 cells ($P < 0.001$). On the other hand, silencing of ANXA5 blocked calcium influx (Supplementary Fig. 8e, f). Fluo-4 AM detection also showed that inhibition of ANXA5 expression reduced calcium influx in neutrophils compared with the control group (Supplementary Fig. 10g, h).

Inhibition of ANXA5 reduces S100A12-induced NETs formation and alleviates MI injury

To further investigate the role of ANXA5 in S100A12-induced MI injury, AAV-shANXA5 was administered to downregulate the expression of ANXA5 in vivo 3 weeks before MI. The control group was injected with AAV-shNC. Knockdown of ANXA5 had no significant effects on cardiac function in WT mice 3 or 28 days after MI; however, it significantly improved post-infarction cardiac function in TG mice (28 d EF: $P = 0.0084$, 28 d FS: $P = 0.0059$) (Fig. 6a–d). Moreover, we observed decreased apoptosis- and NETs-related protein expression in AAV-shANXA5 treated mice one day after MI (Fig. 6e–g). Inhibition of ANXA5 expression resulted in a lower concentration of double-stranded DNA (dsDNA) in the plasma of AAV-shANXA5 treated TG mice than in the AAV-shNC group ($P = 0.0001$) (Fig. 6h). Immunofluorescence staining also revealed that the expression of the NETs marker (citH3) was significantly reduced in AAV-shANXA5 treated mice than that in AAV-shNC-treated mice in both the WT and TG groups (Fig. 6i, j). Overall, these data demonstrated that ANXA5 inhibition with AAV-shANXA5 reduces the formation of NETs, alleviates the degree of apoptosis, and improves cardiac function after MI.

Hypoxia-inducible factor-1α (HIF1α) governs S100A12 expression under hypoxia and MI injury

We went on to investigate the molecular mechanism of S100A12 induction under MI. HIF1α is the most rapidly induced transcription regulatory factor in neutrophils after hypoxic injury. We evaluated the expression of HIF1α and S100A12 in a time course study. We found that the expression of HIF1α, S100A12, lysozyme, and NET-related proteins
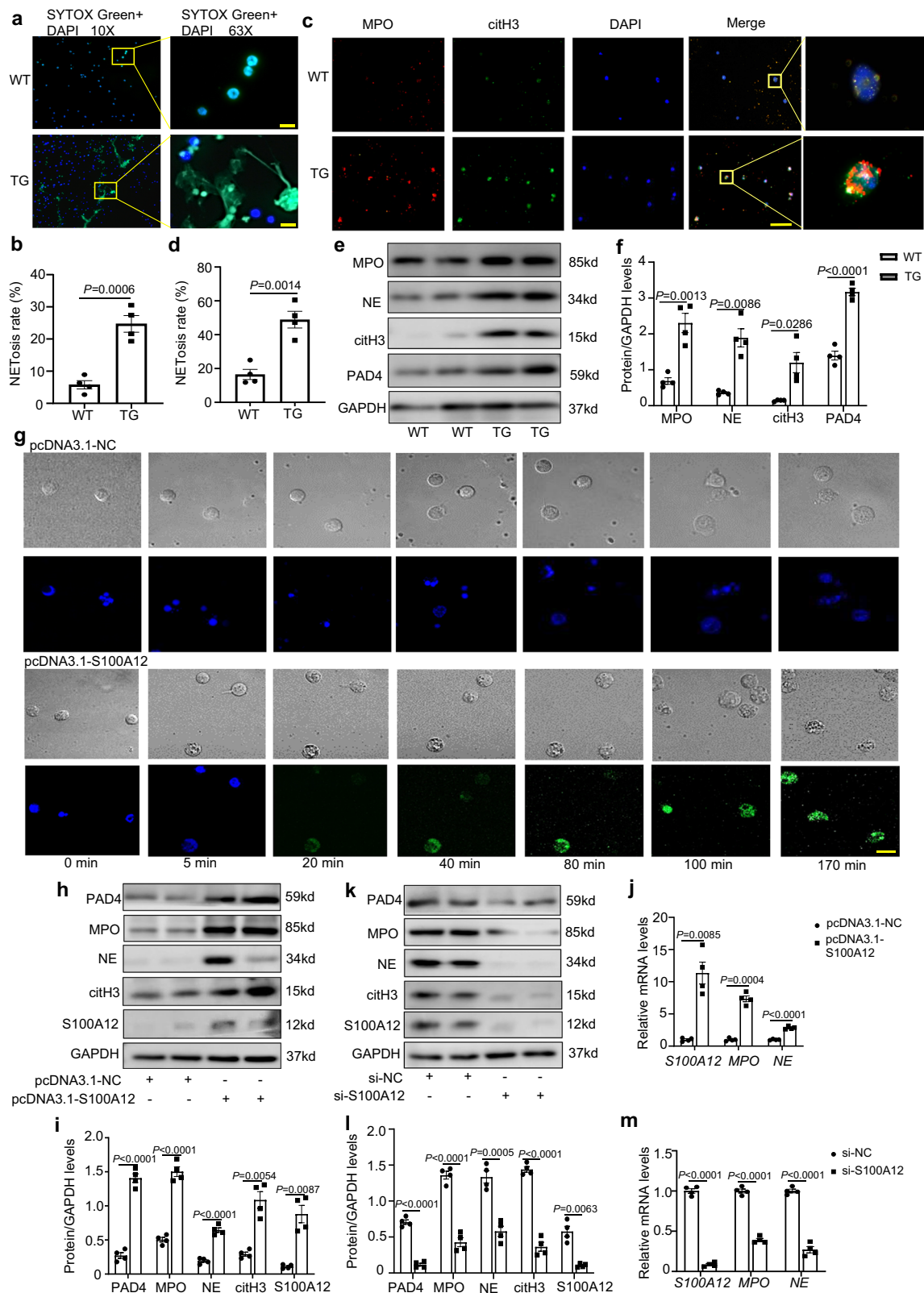
in neutrophils was increased with prolonged hypoxia (Supplementary Fig. 9a, b). In contrast, silencing of HIF1α significantly decreased the expression of S100A12 after hypoxia (Supplementary Fig. 9c–f). Bioinformatics analysis of the S100A12 promoter region identified a HIF1α binding site (Supplementary Fig. 9g). To further evaluate whether HIF1α binds to the promoter of S100A12, we constructed a dual luciferase reporter gene vector containing the promoter of S100A12.

We showed that overexpression of HIF1α significantly increased the promoter activity of S100A12 (Supplementary Fig. 9h).

Plasma dsDNA concentration is associated with S100A12 level in STEMI patients and can predict 1-year prognosis after STEMI

Secreted NETs consist of multiple components, such as granule proteins (NE and MPO) and dsDNA. PAD4 is the most important enzyme

Fig. 3 | Expression of S100A12 led to neutrophil extracellular traps (NETs) formation. Bone marrow-derived neutrophils (BMDNs) were isolated from the WT and TG mice. **a** SYTOX Green staining was performed to observe the rate of NETosis in BMDNs from TG and WT mice. Scale bar, 10 μm. **b** Analysis of NETosis rate ($n = 4$ biological replicates). **c, d** Immunofluorescence double staining and quantification of myeloperoxidase (MPO) and citrullination of histone 3 (citH3) in BMDNs from TG and WT mice. Scale bar, 50 μm. ($n = 4$ biological replicates). **e, f** Representative blots of NETs-related proteins [MPO, neutrophil elastase (NE), citH3, and peptidyl-larginine deiminase 4 (PAD4)] and quantification of TG and WT primary neutrophils. Two-tailed unpaired t-test is used for statistical analyses of MPO and PAD4, unpaired t-test with Welch's correction is used for analyses of NE and Mann-Whitney test is used for analyses of citH3 ($n = 4$ biological replicates). **g** DHL-60 cells transfected with or without pcDNA3.1-S100A12 were monitored using live cell imaging using three parameters: morphology using differential interface contrast (DIC), cell death using the cell-impermeable DNA dye SYTOX Green (green), and chromatin depolymerization using the cell-permeable DNA marker Hoechst 33342 (blue). These were performed in a humidified atmosphere containing 5% CO2 at

37 °C. The cells were monitored every 5 min for 300 min. Important time points are shown in min. Results are representativeof at least 3 independent experiments. Scale bar, 10 μm. **h, i** Western blotting was conducted to detect the protein expression of NETs-related proteins and statistical results for cells transfected with pcDNA3.1-S100A12. Two-tailed unpaired t-test is used for statistical analyses of MPO, PAD4 and NE, and unpaired t-test with Welch's correction is used for analyses of citH3 and S100A12 ($n = 4$ biological replicates). **j** Relative mRNA levels of *S100A12*, *MPO* and *NE* in cells transfected with pcDNA3.1-S100A12. Two-tailed unpaired t-test is used for statistical analyses of *NE*, and unpaired t-test with Welch's correction is used for analyses of *MPO* and *S100A12* ($n = 4$ biological replicates). **k, l** Representative blots of NETs-related proteins and quantification in dHL-60 cells transfected with si-S100A12. Two-tailed unpaired t-test is used for statistical analyses of MPO, PAD4, NE and citH3, and unpaired t-test with Welch's correction is used for analyses of S100A12 ($n = 4$ biological replicates). **m** Relative mRNA levels of *S100A12*, *MPO* and *NE* in cells transfected with si-S100A12. Data are expressed as mean ± SEM. Statistical analyses were carried out using two-tailed unpaired t-test for (**b**), (**d**) and (**m**). Source data are provided as a Source Data file.

that induces histone deamination during NET formation. Therefore, we analysed the association between S100A12 levels and dsDNA, NE concentration, and PAD4 enzyme activity in STEMI patients. We found that the plasma concentration of S100A12 was significantly correlated with the level of dsDNA ($r = 0.607$, $P < 0.0001$), whereas there was no significant correlation between S100A12 and NE plasma concentration ($r = 0.243$, $P = 0.0004$) or PAD4 enzyme activity ($r = -0.021$, $P = 0.2743$) (Fig. 7a–c).

Next, patients in this cohort were stratified according to the baseline tertile of plasma dsDNA levels (Table 1). Diabetes, hscTnT, and dsDNA concentrations were higher in patients with high plasma dsDNA levels, whereas other baseline characteristics were unrelated to dsDNA. During the 1-year clinical follow-up, Major Adverse Cardiovascular and Cerebrovascular Events (MACCE) rate was at the top in patients in the highest peak dsDNA tertile, intermediate in the middle tertile, and the least in the lowest tertile. Moreover, higher peak plasma dsDNA levels were associated with increased risk of all-cause mortality (Table 2).

Discussion

This study demonstrated that hypoxia-induced S100A12 expression in neutrophils rapidly stimulated the generation of NETs by increasing the ANXA5-calcium axis, which exacerbated MI and poor prognosis (Supplementary Fig. 10). Blockage of S100A12-ANXA5-calcium overload axis effectively attenuated the impairment of heart function after AMI. Detecting changes in NETs components in the plasma of patients with early AMI might indicate poor prognosis.

MI induces a massive systemic inflammatory response, evidenced by increased infiltration of inflammatory cells into the ischemic heart[17]. Neutrophils are the main early responder cells recruited to the myocardial infarct zone throughout the first 24–48 h post-AMI[18]. Activated neutrophils are rapidly mobilized into the heart tissue and participate in the repair of inflammatory damage through neutrophil kinetics and secrete an array of proteolytic and oxidative substances through NETosis, a form of cell death recent reported, which involving the extrusion of decondensed chromatin along with its complete granular content[19]. In response to an array expanding stimuli, NETs are extruded by activating or dying neutrophils that comprise decondensed chromatin and decorated with various protein mediators, including histones, granule proteins (including NE and MPO), and cytosolic proteins (including S100 calcium-binding proteins A8, A9, and A12, as well as actin and α-actinin)[15,19]. Therefore, targeting neutrophil kinetics or NET production may represent a promising approach for reducing the degree of inflammation and reperfusion injury that occurs after AMI[20].

The present study investigated whether neutrophil recruitment into the infarct zone and surrounding areas is a main feature of

ischemic cardiac injury 24 h post-MI and whether neutrophils are causally associated with ischemia-induced myocardial damage and NETs formation. Furthermore, we demonstrated that blocking of NETs formation significantly reduced the occurrence of myocardial apoptosis and cardiac dysfunction.

S100A12 (calgranulin C) is a member of the S100 family and is expressed in considerable amounts almost exclusively by granulocytes[21]. Human S100A12 is a proinflammatory factor that enhances proinflammatory responses at sites of inflammation[22]. Our previous study showed that the serum concentration of S100A12 rapidly increased, especially within the first 2 h after symptom onset, in patients with STEMI[9]. *In present study, we found that S100A12 expression peaked within 1 d after MI and subsequently declined, suggesting that the elevation of S100A12 is mainly concentrated in the early stage of MI injury. Moreover, we showed that S100A12 expression in neutrophils exacerbated cardiac functional impairment in mice after early MI, increasing apoptosis in heart tissue by elevating cytoplasmic and mitochondrial Ca^{2+} concentration, which promoted suicidal NETosis formation. In addition to its role of initiating leukocyte dynamics and NETosis, other studies suggest that S100A12 may lead to an abnormal increase in MMPs activity by modulating Zn^{2+} [23,24] and promoting atherogenesis.*

Proteomic analysis and cytological experiments confirmed that ANXA5 is a vital molecule involved in S100A12-mediated NETs formation. Both in vivo and cytological studies have confirmed that the inhibition of ANXA5 can significantly suppress S100A12-induced NETosis and cardiac function damage after MI. Interestingly, annexins and S100 proteins represent two large but distinct calcium-binding protein families. Annexins comprise a large α-helical core domain that binds calcium ions and enables their interaction with phospholipid membranes. Furthermore, some annexins, including A1 and A2, contain an N-terminal region that is excluded from the core domain upon calcium binding[25]. These features enable interaction of the annexin N-terminus with target proteins, including S100. Structural studies of the complexes between the members of these two families have revealed valuable details regarding the mechanisms of the interactions, including the binding surfaces and conformation of the annexin N-terminus[26]. However, an interaction between S100A12 and ANXA5 has not yet been reported. We performed immunoprecipitation analysis and confirmed the interaction between S100A12 and ANXA5. Additionally, immunofluorescence staining revealed that S100A12 enhances the cell membrane translocation effects of ANXA5, which may be involved in the calcium-induced formation of NETs. *Future experimental studies will employ structural biology approaches, such as X-ray crystallography or cryo-electron microscopy, to map the binding interface between S100A12 and ANXA5. Additionally, functional assays using site-directed mutagenesis could clarify how this interaction regulates calcium signaling and NETs production. Elucidating these details*
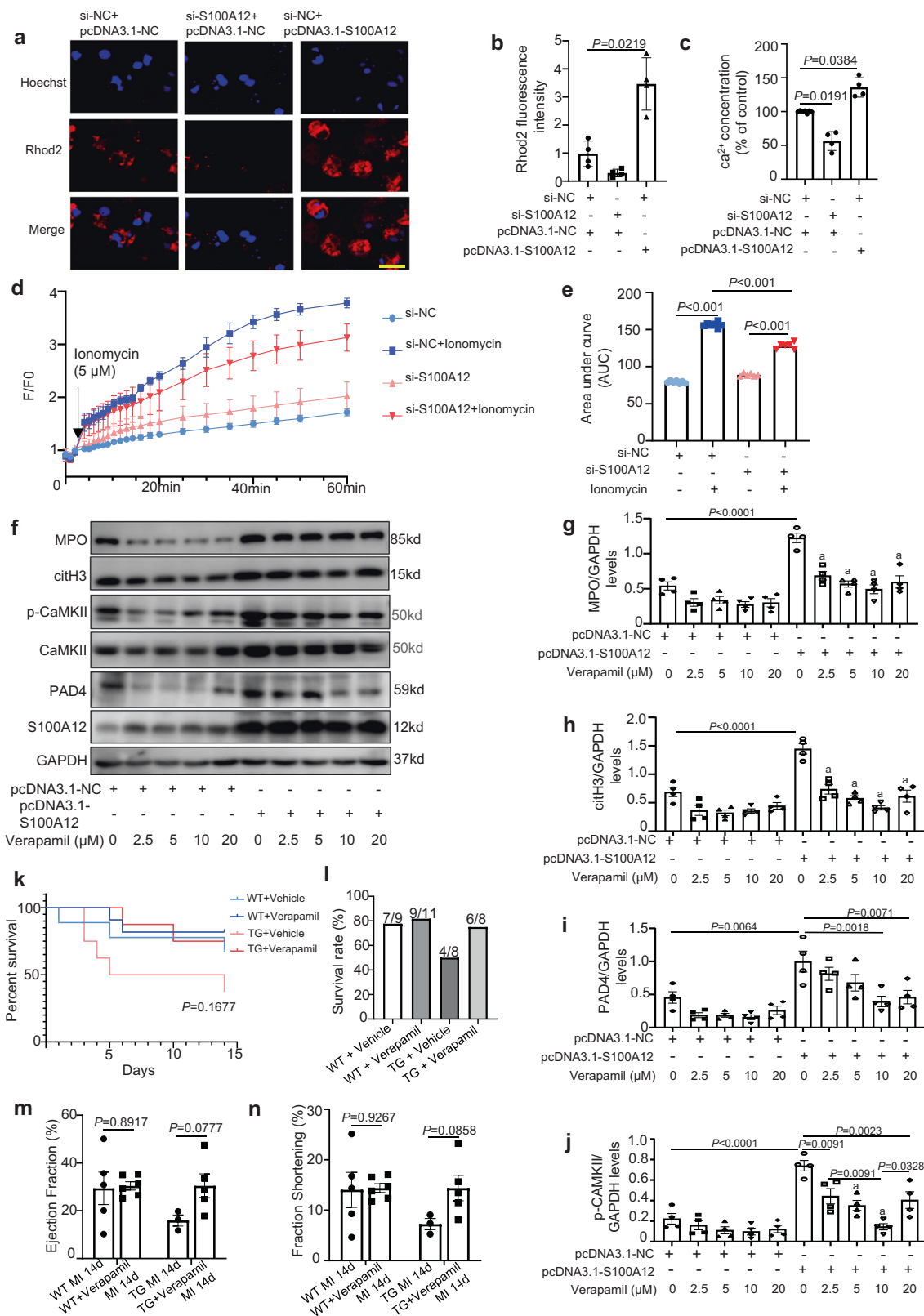
will deepen our understanding of the signaling pathways involved and may uncover novel therapeutic targets.

Several studies reported that treatment with the calcium iono-phores ionomycin and A23187[27,28] leads to NETs release[29]. Notably, extracellular calcium chelation inhibits NETosis, while intracellular calcium chelation impairs NETosis induced by IL-8, PMA, and nigericin[30,31]. Thus, an increase in intracellular calcium through either releasing intracellular stores or influx from the extracellular environment is crucial for NETosis. However, the cellular processes requiring calcium during NETosis remain unclear. In present study, we identify that regulating calcium ion influx can trigger the occurrence of NETs, which is mediated by the direct interaction between S100A12 and ANXA5. Consistently, we also observed that blocking calcium ion entry effectively inhibited NETs formation, which implied that Ca^{2+} signalling

Fig. 4 | Endogenous S100A12 induced neutrophil extracellular traps (NETs) formation by calcium influx overload. a, b Intracellular calcium concentration detected by confocal Rhod2 staining, and statistical results after transfection of si-S100A12 or pcDNA3.1-S100A12 ($n = 4$ biological replicates). Scale bar, 10 μm. **c** Colorimetric detection of intracellular Ca^{2+} concentration in dHL-60 cells transfected with pcDNA3.1-S100A12 or si-S100A12 ($n = 4$ biological replicates). **d, e** Neutrophils transfected with or without si-S100A12 were preloaded with calcium probe Fluo-4 AM dye and incubated for 30 min in HBSS calcium-free media. After washing, cells were resuspended in Assay Buffer and stimulated with ionomycin (5 μM). Time-course of fluorescent signal was recorded with excitation and emission wavelengths of 488 and 526 nm, respectively. The fluorescence was normalized to the baseline fluorescence F0 (fluorescence measurement at the first time point). The Area under curve (AUC) was estimated using sums-of-squares method ($n = 6$ biological replicates). **f–j** Representative blots of peptidylarginine deiminase 4 (PAD4), p-CaMKII, myeloperoxidase (MPO), citrullination of histone 3 (citH3) and

quantification in dHL-60 cells treated with pcDNA3.1-S100A12 and different concentration of calcium channel blocker (Verapamil) ($n = 4$ biological replicates). a: $P < 0.0001$ vs pcDNA3.1-NC + 0 μm Verapamil. **k, l** Mice were intraperitoneally injected with corn oil or Verapamil (5 mg/kg/d) every other day from Day 1 before the MI operation to post-MI Day 3. Survival curves and rates of WT and TG mice treated with Verapamil for 14 days after MI were analyzed using Log-rank (Mantel-cox) test. **m, n** Echocardiographic parameters were analyzed in WT and TG mice treated with verapamil at post-MI Day 28 ($n = 5$ biological replicates for WT MI group, $n = 6$ biological replicates for WT + Verapamil group, $n = 3$ biological replicates for TG MI group and $n = 5$ biological replicates for TG + Verapamil group). Data are expressed as mean ± SEM. Statistical analyses were carried out using two-tailed unpaired t-test for (**m**), (**n**), one-way ANOVA with Tukey's multiple comparisons test for (**e**), (**g**), (**h**), (**i**), (**j**) and Brown-Forsythe and Welch's ANOVA test for (**b**), (**c**). Source data are provided as a Source Data file.

is necessary for several vital processes that are fundamental to neutrophil function. *The S100A12-ANXA5-calcium axis shows significant potential for anti-inflammation and protection against the myocardial injury post MI. Evaluating pharmacologic inhibitors targeting the S100A12-ANXA5-calcium axis or the S100A12-ANXA5 interaction may provide valuable translational insights. Further studies are required to elucidate the regulatory mechanisms and signalling pathways involved in the S100A12-ANXA5 interaction.*

Neutrophils are well-known to promote myocardial injury through ROS, granular components, and pro-inflammatory mediators. Recent and our study show that neutrophils can form extracellular traps to increase inflammation and cardiac injury, emerging evidence also reveals their critical role in appropriate wound healing after MI. Neutrophils promote inflammation resolution, angiogenesis, and scar formation. Maintaining a time-dependent balance in neutrophils activity—where inflammatory processes are followed by timely resolution and reparative mechanisms—is crucial for successful heart healing and remodeling following MI.

Methods
Detailed materials and methods are described in Supplementary data.

Ethics statement
All animal studies were approved by the Ethics Committee of General Hospital of Northern Theater Command Hospital, and were performed in strict accordance with the Guide lines for the Care and Use of Laboratory Animals published by the US National Institutes of Health. All animals were housed at a constant temperature of 22 °C and humidity of 50% in a 12 h light-dark cycle system with freely available food and water. The written informed consent was obtained from all participants, and the Ethics Committee of General Hospital of Northern Theater Command Hospital approved the study protocols (No. k (2012) 17-1).

Mice
The lysozyme M promoter and S100A12 gene sequence were constructed on the transposon. Briefly, the linearized transgenic vector was injected into the embryonic stem cells of C57BL/6 J pseudo-pregnant females by microinjection to prepare transgenic (TG) mice. Model Animal Research Centre of Nanjing University was commissioned to prepare and breed the TG mice. Our laboratory continued to feed and reproduce them under specific pathogen-free conditions. Male mice of 10-16 weeks old were used. To evaluate the function of S100A12, S100A12-TG mice were divided into two groups: TG Sham group and TG MI group. Cardiac function and morphologic changes were evaluated at 1, 3, 7, 14 and 28 days (d) after MI. DNase I (Pulmozyme, Genentech, USA) was used to decompose the structure of NETs. Post MI mice were randomly assigned to 4 groups: WT+Saline, WT+DNase I, TG+Saline, and TG+DNase I. Mice in each group were injected intraperitoneally with saline or DNase I (10 mg/kg/day) every other

day from Day 1 before MI to Day 3 after surgery. Adeno-associated virus (AAV) carrying shRNA purchased from HanbioTech (HYKY-211214029-DAAV, Shanghai, China) were injected into the tail of mice 3 weeks before MI.

Induction of MI
In brief, animals were randomly assigned to either MI group or sham operated group. All mice were anesthetized with 2% isoflurane gas and fixed in supine position. Whether the mechanical ventilation was successful was judged according to the respiratory motility of the mouse chest and the frequency of small animal ventilator. A small cut was made on the skin between the 3-4 left intercostal space in order to visualize the left ventricle. Subsequently, ligating the left anterior descending (LAD) coronary artery with 6-0 silk suture. Successful occlusion of the blood flow was confirmed by the blanching of anterior wall of left ventricle. After squeezing and pinching the gas out of the chest cavity, the chest wall and the skin at the wound were closed with 4-0 silk suture. The endotracheal tube was detached once spontaneous respiration resumed, and the mice were placed on a heating pad maintained at 37 °C until they were completely awake. The sham operated mice adopted the same procedure without ligating the LAD artery. Mice dying within 24 h of the ligation operation (<10% of all animals) were classified as technical failures and excluded from subsequent analysis.

Assessment of cardiac function
Cardiac function was measured by ultrahigh resolution small animal ultrasound imaging system (Vevo 2100, VisualSonics, Canada) equipped with an MS-400 imaging transducer. After removing the hair on the chest and upper abdomen of mice, the mice were slightly anesthetized with 1% isoflurane inhalation. Heart rate was kept between 500 and 600 beats per minute in all mice. The two-dimensional images of the left ventricle were collected on the left mid-papillary short axis view. At the same time, echocardiography records of 10 cardiac cycles in M-mode under two-dimensional guidance were obtained. Left ventricular end diastolic diameter (LVEDD) and left ventricular end systolic diameter (LVESD) were measured. The manufacturer's software automatically calculated the left ventricular volume in diastole (LVVD), left ventricular volume in systole (LVVS), left ventricular ejection fraction (LVEF%) and left ventricular fractional shortening (LVFS%). Echocardiogram recording and image analysis were performed by a technician who was blinded to treatment groups.

Hematoxylin and eosin (H&E) and Masson staining
After mice were sacrificed under general anesthesia, the hearts were rinsed with chilled phosphate-buffered saline (PBS) and completely immersed in 4% paraformaldehyde for 48 h (h). Heart tissue samples were then dehydrated, embedded in paraffin and sliced into 4 μm thick sections. Histological sections were stained with H&E and Masson's Trichrome staining to determine the morphological effects and infarct
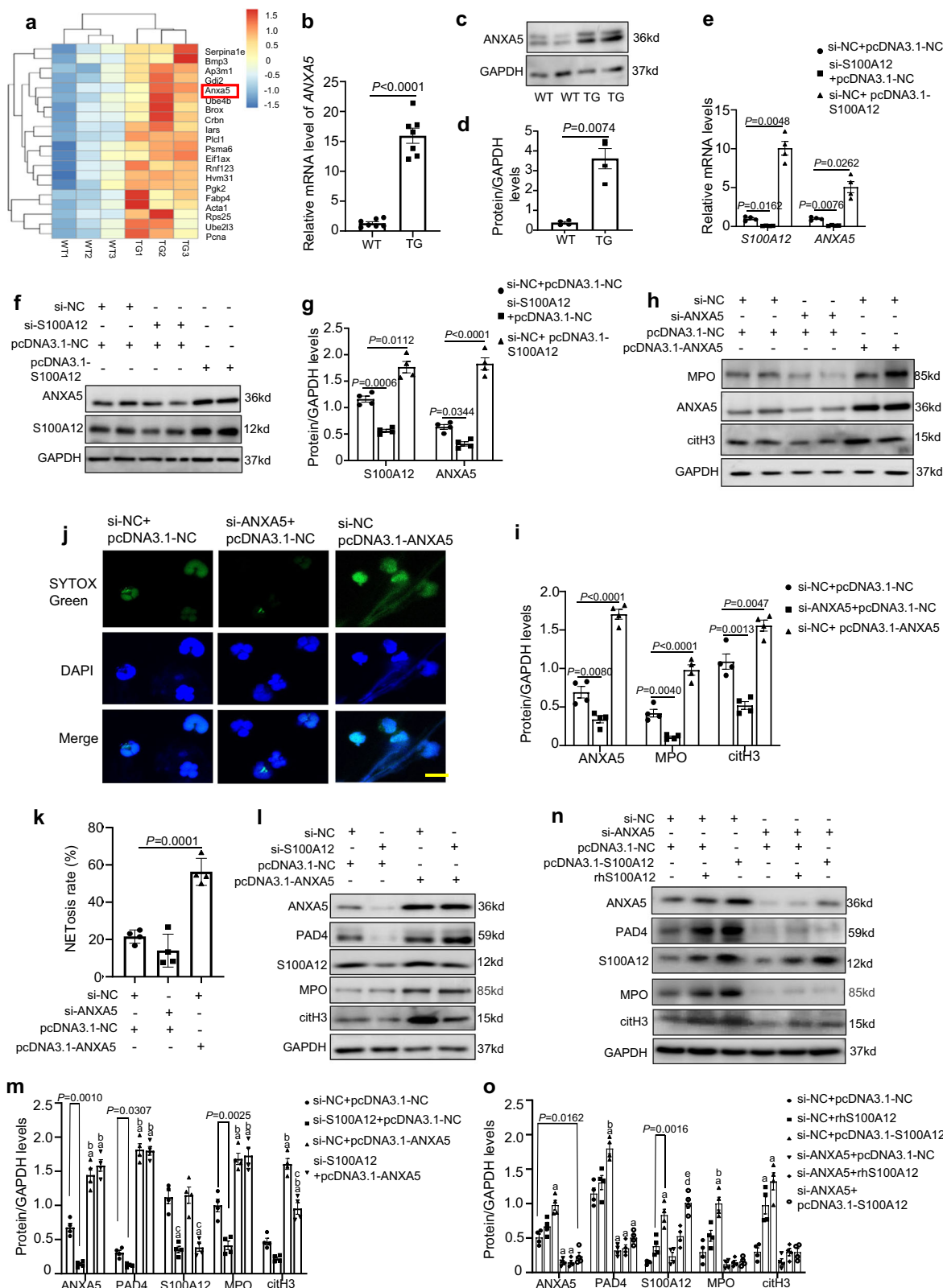
size, which was calculated as the ratio of the infarction length to the perimeter of the left ventricle in each section. The quantification of infarct and fibrosis region was estimated using Image J software.

Immunofluorescent and immunohistochemical (IHC) staining
For immunostaining, heart sections were deparaffinized in xylene for 30 min and rehydrated with alcohols at decreasing concentration (100,

100, 85, 75%). Antigen retrieval was achieved by boiling sections for 40 min in the diluted Antigen Retrieval Buffer (50×EDTA Buffer, pH 8.0, Solarbio, Beijing, China) and cooling down at room temperature for 1 h. After the inhibition of endogenous peroxidase activity with 3% H_2O_2 for 20 min, the sections were then washed with PBS and incubated with 5% bovine serum albumin (BSA) solution for 30 min. Primary antibodies were applied overnight at 4 °C in PBS containing 1% BSA. The next day,

Fig. 5 | Annexin A5 (ANXA5) mediated endogenous S100A12-induced neutrophil extracellular traps (NETs) formation. a Heat map of significantly differentially expressed proteins in WT and TG mice. **b** Relative mRNA levels of *ANXA5* in BMDNs from TG and WT mice (*n* = 7 biological replicates). **c, d** Western blotting was conducted to detect the protein expression of ANXA5 for BMDNs from TG and WT mice and statistical results (*n* = 4 biological replicates). **e** Relative mRNA levels of *ANXA5* in dHL-60 cells transfected with si-S100A12 or pcDNA3.1-S100A12 (*n* = 4 biological replicates). **f, g** Representative blots of ANXA5 and S100A12 and quantification in cells treated with si-S100A12, pcDNA3.1-S100A12, or rhS100A12. One-way ANOVA with Tukey's multiple comparisons test is used for statistical analyses of ANXA5, Brown-Forsythe and Welch's ANOVA test is used for analyses of S100A12 (*n* = 4 biological replicates). **h, i** Representative blots of myeloperoxidase (MPO), citrullination of histone 3 (citH3), ANXA5 and quantification in dHL-60 cells treated with si-ANXA5 or pcDNA3.1-ANXA5 (*n* = 4 biological replicates). **j, k** SYTOX Green staining was performed to observe the rate of NETosis in dHL-60 cells transfected with si-ANXA5 or pcDNA3.1-ANXA5 (*n* = 4

biological replicates). Scale bar, 10 μm. **l, m** Representative blots of MPO, citH3, peptidylarginine deiminase 4 (PAD4) and quantification in dHL-60 cells treated with si-100A12 and pcDNA3.1-ANXA5 (*n* = 4 biological replicates). One-way ANOVA with Tukey's multiple comparisons test is used for statistical analyses of ANXA5, S100A12, MPO and citH3, Brown-Forsythe and Welch's ANOVA test is used for analyses of PAD4. a: $P < 0.01$ vs si-NC + pcDNA3.1-NC, b: $P < 0.01$ vs si-S100A12 + pcDNA3.1-NC, c: $P < 0.01$ vs si-NC + pcDNA3.1-ANXA5. **n, o** Representative blots of MPO, citH3, PAD4 and quantification in dHL-60 cells treated with si-ANXA5 and pcDNA3.1-S100A12 with changes in exogenous S100A12 content (*n* = 4 biological replicates). a: $P < 0.01$ vs si-NC + pcDNA3.1-NC, b: $P < 0.01$ vs si-NC + rhS100A12, c: $P < 0.01$ vs si-NC + pcDNA3.1-S100A12, d: $P < 0.01$ vs si-ANXA5 + pcDNA3.1-NC, e: $P < 0.01$ vs si-ANXA5 + rhS100A12. Data are expressed as mean ± SEM. Statistical analyses were carried out using two-tailed unpaired *t*-test with Welch's correction for (**b**), (**d**), one-way ANOVA with Tukey's multiple comparisons test for (**i**), (**k**), (**o**) and Brown-Forsythe and Welch's ANOVA test for (**e**), (**c**). Source data are provided as a Source Data file.

the sections were rinsed with PBS and then sequentially incubated with secondary antibody. The peroxidase reaction was visualized using 3,3'-diaminobenzidine tetrahydrochloride (DAB) and sections were counterstained with hematoxylin.

Immunofluorescence staining was performed according to reported procedures at our laboratories. Briefly, tissue sections were permeabilized 10 min in 0.2% Triton X-100 and then blocked with 5% BSA for 30 min at room temperature, followed by incubation with diluted primary antibody overnight at 4 °C. The sections were then stained with fluorescence-conjugated secondary antibody (1:200 dilution, Invitrogen, Carlsbad, CA, USA) for 1 h at 37 °C. Images were captured with an Olympus DX51 fluorescence microscope (Tokyo, Japan) after the cell nuclei were stained with 4',6-diamidino-2-phenylindole (DAPI, Invitrogen, Carlsbad, CA, USA). For each heart sample, at least 4 random fields were measured.

TdT-mediated dUTP nick end labeling (TUNEL) staining
Hearts were collected, embedded in optimum cutting temperature (OCT) compound (Sakura Finetek, Inc., Torrance, USA), rapidly frozen in liquid nitrogen and cut into 4 μm sections. TUNEL staining was performed with In Situ Cell Death Detection Kit (Cat.11684817910, Roche Diagnostics, Indiana, USA), according to the manufacturer's instructions. Nuclei were further stained with DAPI. Images were acquired with fluorescence microscope and TUNEL positive cells were determined as percentage of the total number of nuclei.

RNA isolation and quantitative Real-time PCR (qPCR) Analysis
Total RNA was extracted using the TRIzol reagent (Thermo Fisher Scientific, Waltham, MA, USA). According to the manufacturer's instructions, isolated RNA (1 μg) was subsequently reverse transcribed into complementary deoxyribonucleic acid (cDNA) using a PrimeScript RT reagent Kit with gDNA Eraser (Takara, Tokyo, Japan). qPCR reaction was performed using SYBR Green Master Mix (Takara, Tokyo, Japan) on a Bio-Rad CFX96 PCR System. The primers were purchased from Sangon Biotech (Shanghai, China). The 18S ribosomal RNA levels were used as an internal control. Relative mRNA expression levels of target protein to paired controls were determined using the 2-ΔΔCt method. The primer sequences are described in Supplementary Table 1.

Western blotting
Proteins were extracted from heart tissues or cells using RIPA Lysis and Extraction Buffer (Thermo Fisher Scientific, Waltham, MA, USA) containing protease inhibitor cocktail (Roche Diagnostics, Indiana, USA) and quantified with BCA Protein Assay Kit (Thermo Fisher Scientific, Waltham, MA, USA). Equal amounts of protein from each group were separated on sodium dodecyl sulphate polyacrylamide gel electrophoresis (SDS-PAGE) and then transferred to

polyvinylidene difluoride (PVDF) membranes (Millipore, Billerica, MA, USA). After 5% milk (BD Biosciences, San Jose, CA, USA) in TBST blocking for 1 h, the membranes were incubated with primary antibodies at 4 °C overnight. The next day, blots were incubated with corresponding horseradish peroxidase (HRP)-conjugated secondary antibodies for 1 h after washing with TBST. Images were captured by enhanced chemiluminescence (ECL) reagent (Millipore, Billerica, MA, USA) and quantified using Image J software. Uncropped blots can be found in the Source Data file.

Co-Immunoprecipitation (Co-IP)
The neutropil-like differentiated HL-60 cells were homogenized and lysed with IP lysis buffer (Thermo Fisher Scientific, Waltham, MA, USA) on ice, then centrifuged at 4 °C for 15 min. The protein was incubated with protein A/G agarose (Thermo Fisher Scientific, Waltham, MA, USA) and gently rotated overnight at 4 °C. After extensive washing with IP lysis buffer, the beads were resuspended in a 2× loading buffer and boiled. Target proteins were separated by SDS-PAGE and detected by western blotting method.

Measurement of intracellular Ca^{2+}
The intracellular Ca^{2+} concentration was detected by a Calcium Colorimetric Assay kit (Beyotime, Shanghai, China). In briefly, the dHL-60 cells were lyzed with lysate buffer. Then 75 μL Chromogenic Reagent and 75 μL Calcium Assay Buffer were added to the 50 μL cell lysates, followed by the 10 min incubation. At last, the 96-well microplate reader was used to measure the absorbance at 575 nm.

Fluo-4 AM is one of the most commonly used fluorescent probes for detecting intracellular calcium ion. Cells were stained with Fluo-4 AM dye (Beyotime, Shanghai, China) at 37 °C for 30 min, and then washed and resuspended in Assay Buffer. Fluorescence intensity was determined using a fluorescence spectrophotometer with excitation and emission wavelengths of 488 nm and 526 nm every 1 min. For time course measurements, the fluorescence intensity was normalized to the baseline fluorescence F0 (fluorescence measurement at the first time point).

To observe Ca^{2+} influx in neutrophils, a specific dye for intracellular Ca^{2+} uptake, Rhod-2 (Thermo Fisher Scientific, Waltham, MA, USA) was employed. Briefly, a stock solution of Rhod-2 was dissolved in DMSO, and cells were incubated with Rhod-2 at a concentration of 5 uM at 37 °C in the dark for 30 min. Cells were washed three times to remove excess or non-specific probes. The cells were then observed using a confocal microscope (LSM800, Carl Zeiss Microscopy Ltd, Cambridge, MA).

Detection of double-stranded DNA (dsDNA) concentration
The Quant-iT PicoGreen dsDNA assay kit (Thermo Fisher Scientific, Waltham, MA, USA) was used according to the manufacturer's
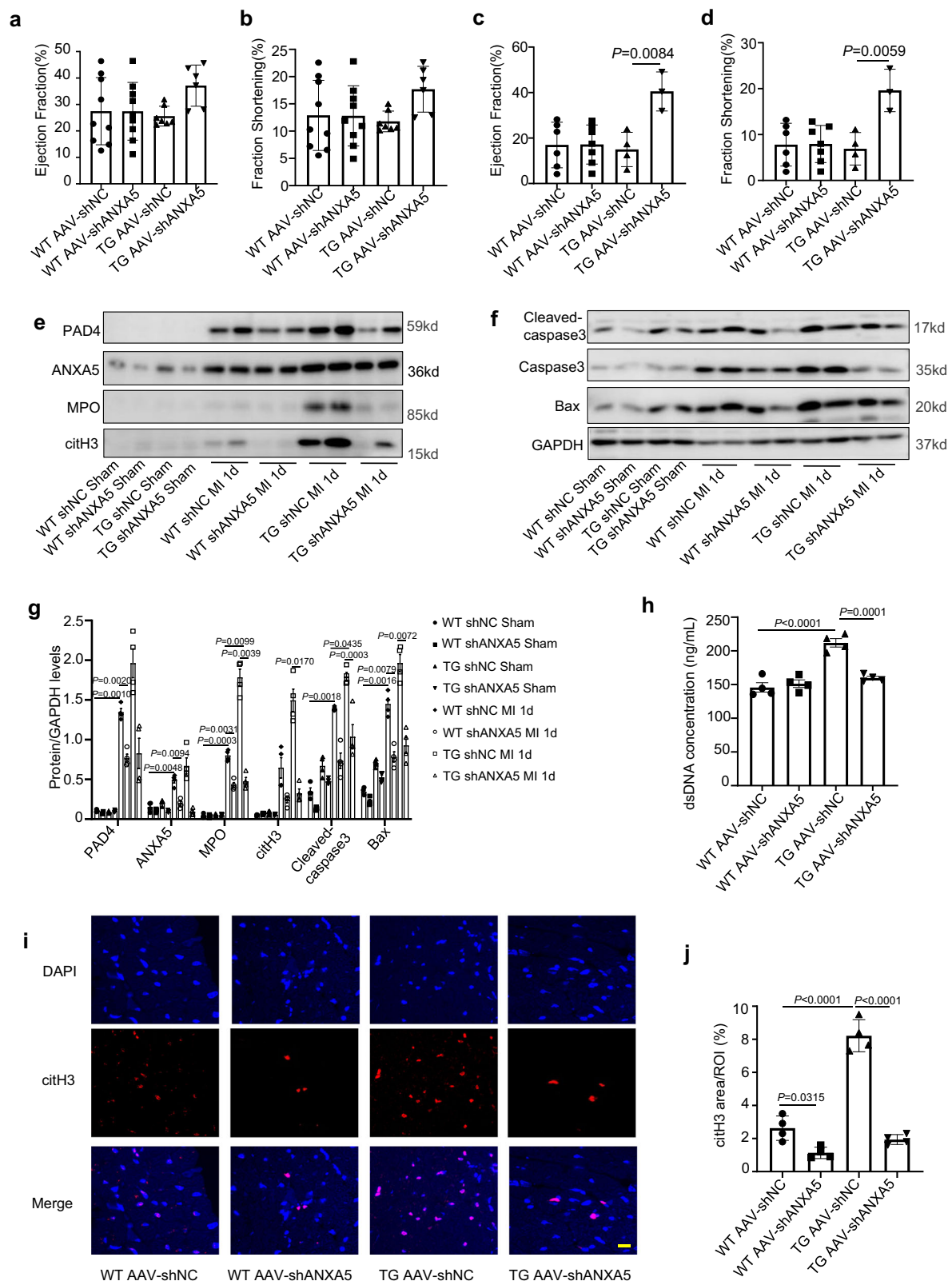
instructions. In brief, we prepared a 5-point standard from 1 ng/mL to 1 μg/mL by serial dilutions. Standards or samples (50 μL) were loaded into black 96-well plates followed by adding 50 μL of the working solution of the Quant-iT PicoGreen reagent to each sample, then incubated for 5 min at room temperature, protected from light. The fluorescence (emission at 485 nm wavelength) intensity was quantified with a fluorescence reader.

Isolation of bone marrow derived neutrophils (BMDNs)

BMDNs were harvested from the tibias and femurs of adult mice. Euthanize the mice and disinfect them. Remove the femurs and tibias, and trim off the epiphyses. Rinse the bone marrow cavities with culture medium containing antibiotics (double antibiotics), passed through 100 μm sterile nylon filters and then centrifuged. Suspension of cells was added onto the Percoll gradient (GE Healthcare, Uppsala, Sweden)

Fig. 6 | Inhibition of Annexin A5 (ANXA5) expression reduced S100A12-induced neutrophil extracellular traps (NETs) formation and alleviated myocardial infarction (MI) injury. a, b Echocardiographic parameters were analyzed in WT and TG mice pre-injected with AAV-shANXA5 or AAV-shNC at Day 3 after MI (*n* = 9 biological replicates for WT AAV-shNC and WT AAV-shANXA5 group, *n* = 7 biological replicates for TG AAV-shNC group and *n* = 6 biological replicates for TG AAV-shANXA5 group). **c, d** Echocardiographic parameters were analyzed in WT and TG mice pre-injected with AAV-shANXA5 or AAV-shNC at Day 28 after MI (*n* = 6 biological replicates for WT AAV-shNC group, *n* = 7 biological replicates for WT AAV-shANXA5 group, *n* = 4 biological replicates for TG AAV-shNC group and *n* = 3 biological replicates for TG AAV-shANXA5 group). **e–g** Representative blots of NETs-

and apoptosis- related proteins, and quantification in WT and TG mice pre-injected with AAV-shANXA5 or AAV-shNC at Day 1 after MI (*n* = 4 biological replicates). **h** Measurements of plasma double-stranded DNA (dsDNA) concentration in WT and TG mice pre-treated with AAV-shANXA5 or AAV-shNC at Day 1 after MI (*n* = 4 biological replicates). **i, j** Immunofluorescence staining of citH3 in WT and TG mice pre-treated with AAV-shANXA5 or AAV-shNC at Day 1 after MI (*n* = 4 biological replicates). Scale bar, 10 μm. Data are expressed as mean ± SEM. Statistical analyses were carried out using one-way ANOVA with Tukey's multiple comparisons test for (**c**), (**d**), (**h**), (**j**), Brown-Forsythe and Welch's ANOVA test for (**a**), (**g**), and Kruskal-Wallis test with Dunn's multiple-comparison test for (**b**). Source data are provided as a Source Data file.
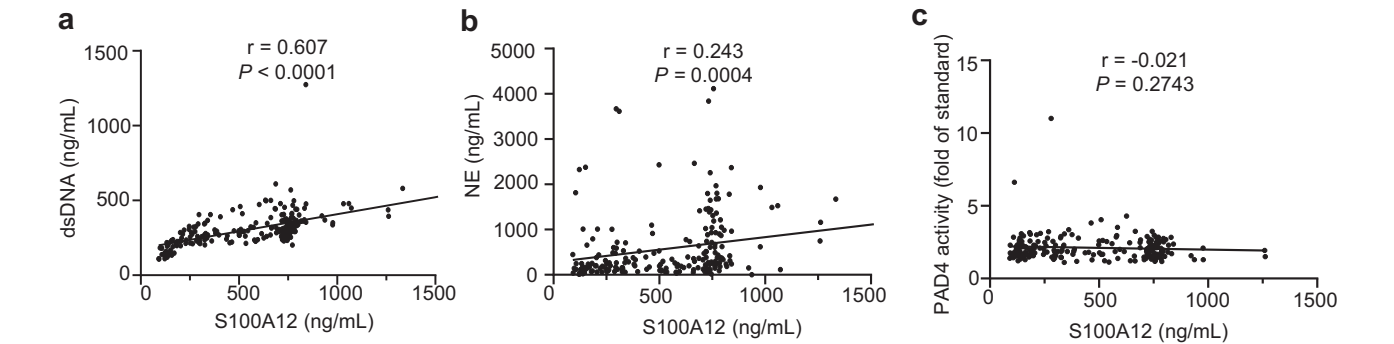

Fig. 7 | Correlation analysis between plasma S100A12 level and markers of neutrophil extracellular traps (NETs) in ST segment elevation myocardial infarction (STEMI) patients. Scatter plots and regression analysis between S100A12 level and double-stranded DNA (dsDNA) concentration (**a**), neutrophil elastase (NE) concentration (**b**) and peptidylarginine deiminase 4 (PAD4) enzyme activity (**c**) in the plasma of STEMI patients. *n* = 230. Pearson's correlation analysis was used. Source data are provided as a Source Data file.

Table 1 | Baseline characteristics of ST segment elevation myocardial infarction (STEMI) patients stratified by double-stranded DNA (dsDNA) tertiles

Variable	Overall (*n* = 230)	Plasma dsDNA levels on admission			*P*-value
		Lowest tertile (*n* = 76)	Middle tertile (*n* = 76)	Highest tertile (*n* = 78)	
Sex, male	191 (83.0)	60 (78.9)	65 (85.5)	66 (84.6)	0.50
Age, years	58.3 ± 12.8	57.3 ± 13.7	57.0 ± 11.9	60.4 ± 12.8	0.18
Hypertension	114 (49.6)	35 (46.1)	43 (56.6)	36 (46.2)	0.33
Current smoking	142 (61.7)	50 (65.8)	45 (59.2)	47 (60.3)	0.07
Diabetes	53 (23.0)	14 (18.4)	18 (23.7)	21 (26.9)	0.45
Previous stroke	24 (10.4)	7 (9.2)	6 (7.9)	11 (14.1)	0.41
TG, mmol/dl	1.8 ± 1.8	1.9 ± 1.0	2.0 ± 1.8	1.6 ± 0.9	0.13
LDL-C, mmol/dl	3.1 ± 0.8	3.0 ± 0.7	3.0 ± 0.8	2.9 ± 0.7	0.71
HDL-C, mmol/dl	1.0 ± 0.2	1.0 ± 0.2	1.0 ± 0.3	1.0 ± 0.2	0.96
GLU, mmol/dl	8.1 ± 3.0	7.9 ± 3.3	9.0 ± 4.6	9.0 ± 6.0	0.23
WBC, 10^9/L	11.5 ± 3.9	11.8 ± 3.3	12.3 ± 3.4	12.2 ± 3.7	0.63
hscTnT, ng/ml	0.9 ± 1.8	0.5 ± 1.2	0.6 ± 1.5	0.7 ± 1.3	0.77
Hs-CRP, mg/l	5.7 ± 9.1	14.3 ± 33.3	11.5 ± 22.9	13.2 ± 31.6	0.73
CK-MB, U/L	56.8 ± 79.9	79.3 ± 112.4	210.0 ± 195.1	246.7 ± 175.5	<0.01
S100A12, ng/ml	551.8 ± 309.0	299.0 ± 217.4	553.9 ± 194.7	779.8 ± 291.0	<0.01
dsDNA, ng/ml	304.1 ± 115.0	203.5 ± 41.1	289.1 ± 20.8	418.2 ± 118.4	<0.01

layers and centrifuged. The cells between 65% and 78% concentration layer were drawn out and lysed with RBC lysis buffer.

Cell culture, transfection, and reporter assays

HL-60 cell line was purchased from the Chinese Academy of Sciences Shanghai Institute for Cell Resource Center and cultured in RPMI 1640 medium (gibco, life technologies corporation, Gaithersburg, MD, USA) containing 20% fetal bovine serum (FBS). HL-60 cells can differentiate into terminally mature neutrophil-like cells via 1.3 % dimethyl sulfoxide (DMSO) induction. siRNA (RiboBio, Guangzhou, China) was

transfected into cells using lipofectamine RNAi max (Invitrogen, Grand Island, NY, USA) and overexpression plasmids of certain gene (GENE-WIZ, Suzhou, China) were transfected with Lipofectamine 2000 (Invitrogen, Grand Island, NY, USA).

For reporter assays, 293 T cells were transfected with luciferase reporter plasmids and overexpression plasmids of target promoter as indicated. Renilla luciferase expression vector pRL-TK was co-transfected as the internal control. The luciferase activity in the cell lysates was determined using the luciferase assay kit (Promega, Madison, WI, USA) and calculated as relative expression to the empty

Table 2 | One-year clinical outcomes in ST segment elevation myocardial infarction (STEMI) patients according to double-stranded DNA (dsDNA) tertiles

Endpoint	Lowest tertile	Middle tertile	Highest tertile
Major Adverse Cardiovascular and Cerebrovascular Events (MACCE)	4	6	8
-All-cause death	1	2	3
-Stroke	2	0	0
-Heart failure	1	2	0
-Reinfarction	0	2	5

vector. The experiment was repeated six times as independent experiments.

ELISA
After 24 h of transfection, cells were replaced with serum-free RPMI 1640 medium. After 24 h, the cell culture supernatant was collected and centrifuged at 4 °C for 20 min. The supernatant concentration of S100A12 was detected using CircuLex S100A12/EN-RAGE ELISA Kit (CY-8058V2, MBL, Japan), according to the manufacturer's instructions. The optical density (OD) of each sample was measured using a spectrophotometer microplate reader at dual wavelengths of 450/540 nm. In addition, the NE concentration and PAD4 activity in the plasma of STEMI patients was measured with Human ELA2/ELANE ELISA Kit (Boster, Wuhan, China) and Human PADI4 ELISA kit (Cusabio, Wuhan, China), according to the manufacturer's instructions.

Quantitative proteomics
The aortic tissues of WT and TG mice were collected ($n = 3$ biological replicates in each group) and frozen in liquid nitrogen. The frozen tissue was ground into powder and sonicated with 8 M urea lysis buffer. Centrifuge at 14,000 g for 20 min, take 5uL of the supernatant for protein quantification, and freeze the rest into −80 °C. Place 100 μg protein sample solution in a centrifuge tube, adjust a final volume of 100 μL with Dissolution Buffer, add 5 μL 200 mM Reducing Reagent and incubate at 55 °C for 1 h. Add 5 μL 375 mM Iodoacetamide solution and incubate for 30 min at room temperature away from light. Transfer to a 10 kD ultrafiltration tube, add 200 μL 100 mM Dissolution Buffer, centrifuge at 14,000 g for 20 min, discard the solution at the bottom of the collection tube and repeat 4 times. Make up the volume to 100 μL with 100 mM Dissolution Buffer. Add 2.5 μL of trypsin per sample and incubate at 37 °C for 14 h. On the next day, wash 3 times with ultrapure water, lyophilize the bottom of the enrichment tube, and redissolve with 100 mM Dissolution Buffer. Pre-separate the labeled peptide mixture by methods such as strong cation exchange chromatography. Divide the peptides into multiple components according to properties like charge to reduce sample complexity. Perform reverse phase liquid chromatography separation on each pre-separated component respectively. Use a EASY-Spray column C18 chromatographic column and elute with an acetonitrile-water gradient to separate the peptides on the column. The separated peptides enter the mass spectrometer in sequence for primary mass spectrometry scanning to obtain information such as the mass-to-charge ratio (m/z) and signal intensity of the peptides. Select peptides with high signal intensity in the primary mass spectrometry for secondary mass spectrometry scanning to further fragment the peptides and obtain the mass-to-charge ratio and intensity information of the fragment ions. Use professional mass spectrometry data analysis software Proteome Discoverer 2.1 to process the mass spectrometry data, including peak identification, peptide identification, quantitative analysis, etc. Compare the mass spectrometry data with the protein database. Identify proteins by matching the peptide sequences, and calculate the relative content of proteins in different samples based on the intensity of the reporter ions labeled by TMT. Conduct bioinformatics analysis on the identified and quantified proteins, such as GO functional enrichment analysis and KEGG pathway analysis, to understand the functions of the proteins and the biological processes they participate in, and explore the biological significance of differentially expressed proteins.

Patients
The present cohort comprised 230 patients diagnosed with STEMI from the General Hospital of Northern Theater Command, Shenyang Liaoning Province, China, between January 2016 and May 2017. Exclusion criteria included patients with known active inflammatory or autoimmune diseases, severe heart failure, hemodynamic instability, suspected myocarditis or pericarditis, diseases of the hematopoietic system, known severe kidney or liver disease, known malignancy, use of immunosuppressant agents, and previous coronary artery bypass graft surgery. To analyze the concentration of S100A12 and its association to the markers of NETs (dsDNA, NE and PAD4), blood samples were obtained at the time of arrival at the emergency department for all patients. and plasma were separated and stored at −80 °C immediately.

All confirmed STEMI patients in this cohort were followed via telephone or outpatient clinic visits at 6 months and 1 year after discharge. The primary outcome was major adverse cardiac and cerebral events (MACCE) at 1 year, a composite of all-cause death, repeat myocardial infarction (MI), stroke, or hospitalization for heart failure. Major secondary outcomes were the individual components of MACCE. MI was defined according to the Third Universal Definition of Myocardial Infarction. Stroke was defined as acute focal dysfunction of the brain, retina, or spinal cord lasting longer than 24 h, or of any duration if focal infarction or hemorrhage was confirmed by neuroimaging. All clinical events were adjudicated by physicians blinded to the biomarker analysis results. This study was approved by ethics committee of all participating centers and all patients signed informed consent.

Statistical analysis
Data are shown as means ± SEM. Statistical analyses were performed using GraphPad Prism software (v8.0). Normality test (Shapiro-Wilk) was performed to determine whether data were normally distributed. If data were normally distributed, Student's t-test was used to compare significant difference between two groups. If data were not normally distributed, Mann-Whitney test was used. Differences among three or more groups were conducted with analysis of variance (ANOVA) followed by post-hoc analysis. A P value of <0.05 was considered statistically significant.

Reporting summary
Further information on research design is available in the Nature Portfolio Reporting Summary linked to this article.

Data availability
The data supporting the findings from this study are available within the manuscript and its supplementary information. The mass spectrometry proteomics data have been deposited to the ProteomeXchange Consortium via the iProX partner repository with the dataset identifier PXD060232. Source data are provided with this paper.

References
1. Frantz, S., Hundertmark, M., Schulz-Menger, J., Bengel, F. & Bauersachs J. Left ventricular remodelling post-myocardial infarction: pathophysiology, imaging, and novel therapies. *Eur. Heart J.* **43**, 2549–2561 (2022).

2. CRZHY, H. Long-term Management of Patients with Myocardial Infarction: An Updated Review. *Cardiol. Discov.* **2**, 241–262 (2022).

3. Wicki, R., Marenholz, I., Mischke, D., Schäfer, B. W. & Heizmann, C. W. Characterization of the human S100A12 (calgranulin C, p6, CAAF1, CGRP) gene, a new member of the S100 gene cluster on chromosome 1q21. *Cell Calcium* **20**, 459–464 (1996).

4. Foell, D. et al. Neutrophil derived human S100A12 (EN-RAGE) is strongly expressed during chronic active inflammatory bowel disease. *Gut* **52**, 847–853 (2003).

5. Oesterle, A. & Bowman, M. A. S100A12 and the S100/Calgranulins: Emerging Biomarkers for Atherosclerosis and Possibly Therapeutic Targets. *Arteriosclerosis, Thrombosis, Vasc. Biol.* **35**, 2496–2507 (2015).

6. Xia, P. et al. Roles of S100A8, S100A9 and S100A12 in infection, inflammation and immunity. *Immunology.* **171** 365–376 (2024).

7. Cao, S. et al. Identification of potential hub genes linked to immune and metabolic alterations in postoperative systemic inflammatory dysregulation. *Front. Immunol.* **14**, 1238774 (2023).

8. Saito, T. et al. S100A12 as a marker to predict cardiovascular events in patients with chronic coronary artery disease. *Circulation J.: Off. J. Jpn. Circulation Soc.* **76**, 2647–2652 (2012).

9. Zhang, X. et al. Utility of S100A12 as an Early Biomarker in Patients With ST-Segment Elevation Myocardial Infarction. *Front Cardiovasc Med.* **8**, 747511 (2021).

10. Beltran, J. V. B., Lin, F. P., Chang, C. L. & Ko, T. M. Single-Cell Meta-Analysis of Neutrophil Activation in Kawasaki Disease and Multisystem Inflammatory Syndrome in Children Reveals Potential Shared Immunological Drivers. *Circulation* **148**, 1778–1796 (2023).

11. Ma, Y. Role of Neutrophils in Cardiac Injury and Repair Following Myocardial Infarction. *Cells* **10**, 1676 (2021).

12. Andreadou, I. et al. Immune cells as targets for cardioprotection: new players and novel therapeutic opportunities. *Cardiovascular Res.* **115**, 1117–1130 (2019).

13. Guasti, L. et al. Neutrophils and clinical outcomes in patients with acute coronary syndromes and/or cardiac revascularisation. A systematic review on more than 34,000 subjects. *Thromb. Haemost.* **106**, 591–599 (2011).

14. Papayannopoulos, V. Neutrophil extracellular traps in immunity and disease. *Nat. Rev. Immunol.* **18**, 134–147 (2018).

15. Brinkmann, V. et al. Neutrophil extracellular traps kill bacteria. *Science* **303**, 1532–1535 (2004).

16. Thiam, H. R., Wong, S. L., Wagner, D. D. & Waterman, C. M. Cellular Mechanisms of NETosis. *Annu. Rev. Cell Developmental Biol.* **36**, 191–218 (2020).

17. Ong, S. B. et al. Inflammation following acute myocardial infarction: Multiple players, dynamic roles, and novel therapeutic opportunities. *Pharm. Ther.* **186**, 73–87 (2018).

18. Vafadarnejad, E. et al. Dynamics of Cardiac Neutrophil Diversity in Murine Myocardial Infarction. *Circulation Res.* **127**, e232–e249 (2020).

19. Metzler, K. D., Goosmann, C., Lubojemska, A., Zychlinsky, A. & Papayannopoulos, V. A myeloperoxidase-containing complex regulates neutrophil elastase release and actin dynamics during NETosis. *Cell Rep.* **8**, 883–896 (2014).

20. Doring, Y., Libby, P. & Soehnlein, O. Neutrophil Extracellular Traps Participate in Cardiovascular Diseases: Recent Experimental and Clinical Insights. *Circulation Res.* **126**, 1228–1241 (2020).

21. Vogl, T. et al. S100A12 is expressed exclusively by granulocytes and acts independently from MRP8 and MRP14. *J. Biol. Chem.* **274**, 25291–25296 (1999).

22. Foell, D. et al. Proinflammatory S100A12 can activate human monocytes via Toll-like receptor 4. *Am. J. Respir. Crit. Care Med.* **187**, 1324–1334 (2013).

23. Goyette, J. et al. Pleiotropic roles of S100A12 in coronary atherosclerotic plaque formation and rupture. *J. Immunol. (Baltim., Md: 1950)* **183**, 593–603 (2009).

24. Jiang, W. et al. Blocking the ERK1/2 signal pathway can inhibit S100A12 induced human aortic smooth muscle cells damage. *Cell Biol. Int.* **41**, 1307–1315 (2017).

25. Gerke, V., Creutz, C. E. & Moss, S. E. Annexins: linking Ca^{2+} signalling to membrane dynamics. *Nat. Rev. Mol. Cell Biol.* **6**, 449–461 (2005).

26. Weisz, J. & Uversky, V. N. Zooming into the Dark Side of Human Annexin-S100 Complexes: Dynamic Alliance of Flexible Partners. *Int. J. Mol. Sci.* **21**, 5879 (2020).

27. De Bont, C. M., Koopman, W. J. H., Boelens, W. C. & Pruijn, G. J. M. Stimulus-dependent chromatin dynamics, citrullination, calcium signalling and ROS production during NET formation. *Biochim Biophys. Acta Mol. Cell Res.* **1865**, 1621–1629 (2018).

28. Gupta, A. K., Giaglis, S., Hasler, P. & Hahn, S. Efficient neutrophil extracellular trap induction requires mobilization of both intracellular and extracellular calcium pools and is modulated by cyclosporine A. *PLoS One* **9**, e97088 (2014).

29. Zhang, B. et al. Role of ORAI calcium release-activated calcium modulator 1 (ORAI1) on neutrophil extracellular trap formation in dairy cows with subclinical hypocalcemia. *J. Dairy Sci.* **105**, 3394–3404 (2022).

30. Parker, H., Dragunow, M., Hampton, M. B., Kettle, A. J. & Winterbourn, C. C. Requirements for NADPH oxidase and myeloperoxidase in neutrophil extracellular trap formation differ depending on the stimulus. *J. Leukoc. Biol.* **92**, 841–849 (2012).

31. Van der Linden, M., Westerlaken, G. H. A., van der Vlist, M., van Montfrans, J. & Meyaard, L. Differential Signalling and Kinetics of Neutrophil Extracellular Trap Release Revealed by Quantitative Live Imaging. *Sci. Rep.* **7**, 6529 (2017).

Acknowledgements

Author contributions

These authors contributed equally: Xi Zhang, Haixu Song. These authors jointly supervised this work: Chenghui Yan, Yaling Han. X.Z., H.X.S., D.L., Y.C., Z.Q.L., X.L.Z., X.J.Z., Y.Z. and Q.M.J. performed experiments. X.Z. and H.X.S. analyzed the data and reviewed the manuscript. Y.L.H. and C.H.Y. designed experiments. X.Z., H.X.S and C.H.Y. wrote the manuscript. Y.L.H. and C.H.Y. are the guarantors of this study.

Competing interests

The authors declare no competing interests.

Additional information

Supplementary information The online version contains supplementary material available at
https://doi.org/10.1038/s41467-025-56978-5.

Correspondence and requests for materials should be addressed to Chenghui Yan or Yaling Han.

Peer review information *Nature Communications* thanks Daniela Cihakova, Meraj Khan and Elisa Liehn for their contribution to the peer review of this work. A peer review file is available.

Reprints and permissions information is available at
http://www.nature.com/reprints